AIAA JOURNAL
Vol. 37, No. 10, October 1999

Probabilistic Approach to Predicting Fatigue Lives of Corroded 2024-T3

J. E. Zamber* and B. M. Hillberry†
Purdue University, West Lafayette, Indiana 47907-1288

The objective of this work was to develop a probabilistic approach to predict fatigue lives of corroded 2024-T3 aluminum tensile specimens. An experimental program was established to corrode fatigue specimens made of a 2024-T3 sheet separately on the longitudinal-transverse (LT) and longitudinal-short (LS) metallurgical planes in a 3.5% sodium chloride solution for 6 and 8 days. The specimens were fatigue tested to fracture, and the corrosion pits that nucleated fatigue cracks were analyzed with an electron microscope. Corroded material from the fractured specimens was polished on the short-transverse plane and the pits were viewed and photographed under a light microscope. The largest 10% of the collected pits were fit to Gumbel extreme-value distributions. These distributions were used in a Monte Carlo simulation in which 1000 pit areas were selected, modeled as circular surface or corner cracks, and treated as initial flaw sizes. Fatigue life predictions were based on crack propagation life by use of the initial flaw sizes from the Monte Carlo simulation. Predicted cumulative distribution functions of fatigue life were within 22% of the experimental cumulative distribution functions for the LS specimens. The method predicted a reasonable distribution of fatigue lives for the 6-day LT specimens but consistently underpredicted the experimental distribution of fatigue lives for the 8-day LT specimens.

Introduction

THE replacement of worldwide aging aircraft fleets is unlikely for some time because of the excessive cost. Therefore, to reliably operate older aircraft into the next century, additional knowledge of the mechanisms and predictive methodologies associated with corrosion and fatigue are required. When corroded structural components are exposed to fatigue loading, crack formation and growth are often accelerated, resulting in a reduced remaining life. The structural aluminum alloy 2024-T3 has been the focus of several studies that investigated the mechanisms and modeling of corrosion pitting. Chen et al.[1] discovered that corrosion pitting of 2024-T3 in 0.5-M NaCl was associated with microgalvanic potential differences between constituent particles and the surrounding aluminum matrix. Further, Burynski et al.[2] corroded polished 2024-T3 aluminum coupons on the longitudinal-transverse (LT) plane and collected scanning electron microscope (SEM) micrographs of the pitted LT surface. Analysis of the micrographs yielded corrosion-pit area data, and the largest of these data were fitted to extreme value distributions. Kondo and Wei[3] investigated the transition from pit growth to mode I crack growth by fatigue testing open-hole specimens of 2024-T3 in 0.5-M NaCl at room temperature. Among other things, the authors observed that fatigue cracks that led to failure usually nucleated from a single pit and that the nucleating pits were typically among the largest pits observed.

The work presented here is an extension of the probabilistic method developed by Laz and Hillberry[4] and uses several of the methods and observations of the corrosion studies mentioned earlier. In this work, 2024-T3 aluminum tensile specimens were corroded in a 3.5% NaCl solution and the resulting corrosion-pitting damage was quantified and modeled as the initial damage state from which fatigue life predictions were made. These predictions were verified with an experimental program in which corroded tensile specimens were tested to fracture.

Materials and Methods

Fatigue Specimen Preparation

Two different width (0.25- and 0.5-in.) standard American Society for Testing and Materials (ASTM) flat test specimens[5] were machined from a 0.1-in.-thick 2024-T3 aluminum sheet (Fig. 1). The aluminum alloy used in this work was manufactured in 1976 and of the same lot as that tested by Virkler et al.[6] To ensure surface finish uniformity, all LT and longitudinal-short (LS) specimen surfaces were polished with 340-, 400-, and 600-grit papers, and polished with 4–8-μm and finally 1-μm diamond lapping compounds.

Because of differences in the severity of pitting between the metallurgical planes,[1] the LT and the LS planes were corroded separately for this work. 0.25-in. tensile specimens (LS specimens) were used in tests in which a 0.75×0.1 in. area of one LS edge was corroded and the other surfaces masked off. Similarly, 0.5-in. tensile specimens (LT specimens) were used for LT pitting tests in which a 1.5×0.5 in. area of one of the LT surfaces was corroded while the other side and both edges were masked. Masking of the surfaces was achieved with Tolber Miccro XP-2000 Stop-Off. A photograph of the polished and the stop-off-coated LS and LT specimens is shown in Fig. 1.

Corroding and Fatigue Testing

There are several methods available for corroding aluminum alloys to be used in pitting studies. Among these are natural exposure, salt spray, immersion, and alternate immersion. Alternate immersion has been shown to accelerate corrosion pitting[7] and was selected as the method of corrosion for this work. Fatigue specimens were corroded in a 3.5% NaCl solution by an alternate immersion machine that operates according to ASTM Standard G44-88 (Ref. 7). The alternate immersion corrosion process alternately immerses specimens in a solution of 3.5% NaCl, by weight, for 10 min and then allows the specimens to dry for the remaining 50 min of the hour in a controlled environment. Several parameters were maintained according to the standard; among these were temperature, relative humidity, and pH.

Nine LS and eight LT specimens were corroded in two separate batches for 6 days by identically prepared NaCl solutions. Nine LS and eight LT specimens were corroded together as a batch for 8 days. After corroding, products of corrosion were removed from the specimen surface by rinsing with deionized water followed by immersion in a solution made according to ASTM Standard G1-90 for cleaning corrosion products from aluminum alloys.[8] The cleaning solution was made by mixing 57.8 ml of 86.5% phosphoric acid with 20.0 g of chromium trioxide and enough deionized water to bring the total solution volume to 1.0 liter. The solution was heated to boiling and each specimen was immersed for 5 min before being rinsed in deionized water and finally with ethanol. All specimens were stored under vacuum until fatigue tested.

Presented as Paper 98-2054 at the AIAA/ASME/ASCE/AHS/ASC 39th Structures, Structural Dynamics, and Materials Conference, Long Beach, CA, 20–23 April 1998; received 26 June 1998; revision received 5 February 1999; accepted for publication 26 February 1999.

*Graduate Research Assistant, School of Mechanical Engineering.
†Professor, School of Mechanical Engineering. Member AIAA.

Table 1 Fatigue testing matrix

Specimen type	Number of tests	S_{max}, MPa ($R = 0.1$, $f = 10$ Hz)
6-day LS	9	220
8-day LS	3	220
8-day LS	6	200
6-day LT	8	220
8-day LT	2	220
8-day LT	6	200

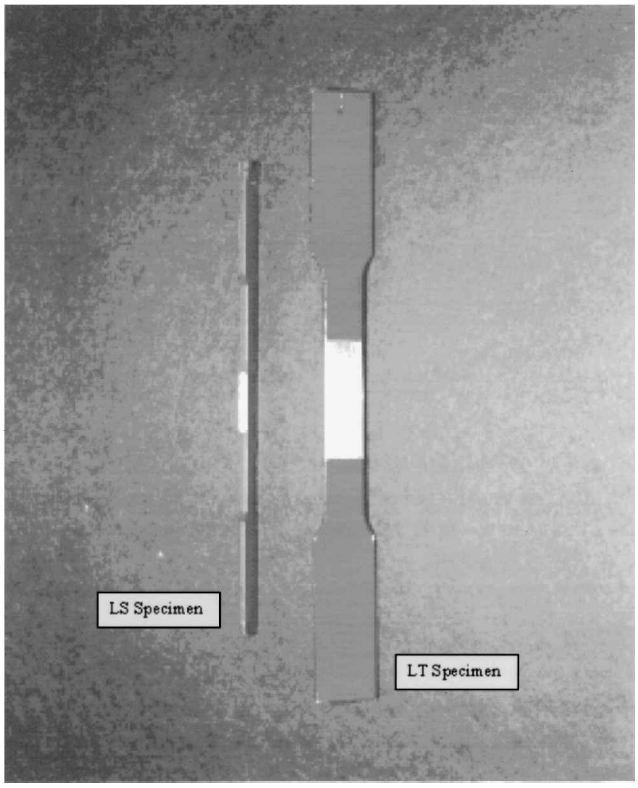

Fig. 1 Polished and Stop-Off-coated LS and LT fatigue specimens.

The corroded specimens were fatigue tested according to the test matrix in Table 1. Fatigue testing was performed with a single-axis load frame with hydraulic wedge grips and a digital closed-loop servohydraulic controller. Initially all tests were to be conducted at a maximum stress of 220 MPa, a stress ratio of 0.1, and a frequency of 10 Hz. The 8-day corroded-specimen maximum stress was reduced from 220 to 200 MPa because of preliminary results that indicated that cracking initiated from multiple nucleation sites. Corroded specimens were cycled until fracture.

Corrosion-Pit Quantification/Fracture Surface Analysis

Methods for corroding and quantifying corrosion-pitting damage in a 0.1-in.-thick 2024-T3 sheet were developed. To ensure that the corroded material used for pitting quantification had the same distribution of pit sizes as the fatigue specimens, corroded material was cut from fatigue specimens after being tested to fracture. The corroded samples used for quantification purposes were mounted in a Buhler Castoglass cold mount with the short-transverse (ST) planes exposed. The ST planes were wet polished with 340-, 400-, and 600-grit papers, a 4–8-μm diamond paste, and finally a 0.01-μm chrome oxide solution. The polished surfaces revealed ST plane projections of the corrosion pits that were viewed with a charge-coupled device (CCD) camera mounted on a light microscope. The CCD images were digitized and saved by a computer and a video acquisition board. Because of the differences in pit sizes, corrosion pits from the 6-day LS specimens were viewed at 800×, whereas all others were viewed at 256×.

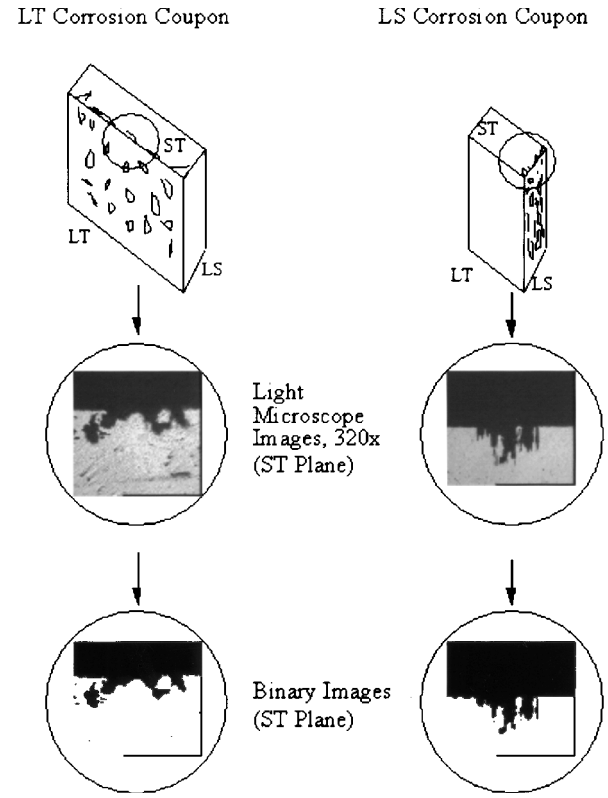

Fig. 2 Schematic of corrosion-pit quantification process for LT and LS coupons.

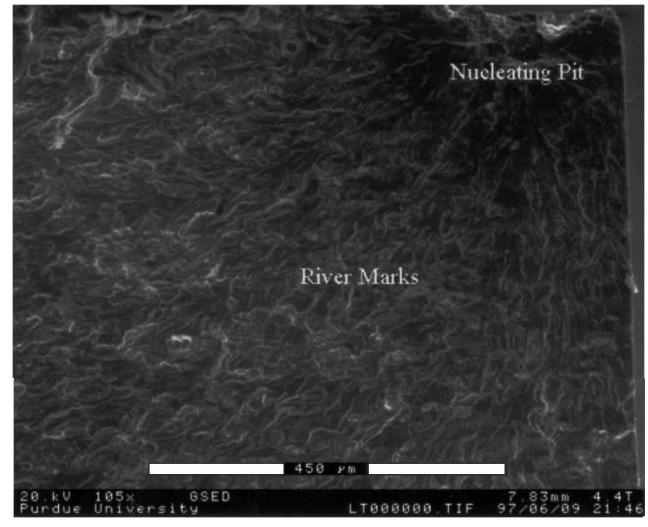

Fig. 3 ESEM micrograph of the nucleating pit: 6-day LT specimen 1.

ST plane projections of corrosion-pit area, maximum depth, and width data were collected through the analysis of the digitized images. The brightness and the contrast of all images were identically adjusted to create binary images, wherein the pits were made black and the surroundings white. The particle analysis tool of the image analysis software, IMIX,[9] was used to count the total number of black pixels to determine pit area. Figure 2 is a schematic representation of the collection procedure.

Pit area measurements were made through analyses of environmental SEM (ESEM) images of the fracture surfaces. Figure 3 is an ESEM micrograph of the fracture surface of a 6-day corroded LT specimen showing, in the upper-right-hand corner, the corrosion pit that nucleated the critical fatigue crack. The nucleating pit was found by a trace of the river marks back to the pit. Another ESEM micrograph taken at higher magnification of the same fracture surface shows the nucleating corrosion pit outlined (Fig. 4).

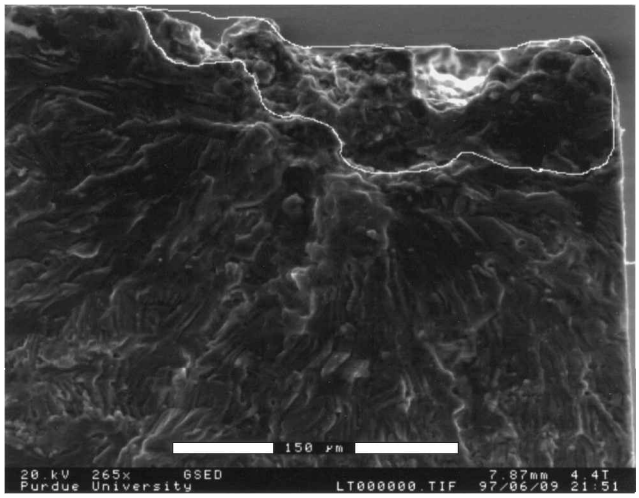

Fig. 4 ESEM micrograph of the nucleating pit outlined: 6-day LT specimen 1.

Each nucleating pit was manually outlined and the area, maximum width, and depth measured with the image analysis software NIH Image.[10]

Probabilistic Model

Assumptions

Assumptions used to simplify, understand, and analyze a physical process are present in any modeling endeavor. The probabilistic model presented here was based primarily on the following assumptions:

1) Corrosion fatigue cracks form at corrosion pits.

2) The cracks that form at the largest pits result in the shortest life.

3) Corrosion pits may be regarded as an initial damage state.

4) Fatigue crack nucleating corrosion pits may be modeled as semicircular surface or corner cracks.

5) Crack nucleation life is small compared with the total life and can be neglected.

6) Fatigue life is based entirely on crack propagation.

Extreme-Value Distributions

Burynski et al.[2] have had success in modeling the largest corrosion pits with type I extreme-value (Gumbel) distributions, the cumulative distribution function of which is given by

$$F_Y(y) = \exp[-\exp[-a(y-w)]] \tag{1}$$

where a and w are obtained from the observed data. Gumbel distributions were fit to the largest 10% of the ST plane projected corrosion-pit area data from each data set. Fitting the distribution involved linearizing Eq. (1) and performing a least-squares fit with the experimental data to obtain the Gumbel distribution parameters a and w. The Gumbel parameters and goodness of fit criteria were calculated and are listed in Table 2. Cumulative distribution functions for each Gumbel fit were plotted with their respective experimental largest pit data sets in Figs. 5 and 6 for the LS and the LT corroded specimens, respectively.

Monte Carlo Simulation

The probabilistic model uses a Monte Carlo simulation to select pit areas from the extreme-value distributions. The assumed fracture mechanics flaw is modeled as a semicircular surface crack with an area equal to that of the selected pit size. A deterministic crack growth model, FASTRAN II, grows the crack to fracture. For each test condition, 1000 pit sizes are randomly selected from the extreme-value distribution and the life is predicted for each. This process is then repeated for each specimen test condition.

Stress-Intensity-Factor Solution

Each pit area generated in the Monte Carlo simulation was modeled as a semicircle, and the radius r was calculated. The initial damage state corresponding to the randomly selected pit area was modeled as either a circular surface crack or a circular corner crack, each of radius r, with stress-intensity-factor solutions by Newman and Raju[11] for elliptical surface or corner cracks for the special case of circularity. The decision to use a corner crack vs a surface crack stress-intensity-factor solution was based on the type of crack that was experimentally favored. The stress-intensity-factor solutions for the surface and corner cracks are of the form given, respectively, by

$$K_I = \frac{\sigma\sqrt{\pi b}}{E(k)} F_s\left(\frac{b}{a}, \frac{b}{t}, \frac{a}{W}, \phi\right) \tag{2}$$

$$K_I = \frac{\sigma\sqrt{\pi b}}{E(k)} F_c\left(\frac{b}{a}, \frac{b}{t}, \phi\right) \tag{3}$$

The process of modeling circular corner cracks from photographed semicircular surface cracks is shown in the schematic representation of Fig. 7.

Table 2 Gumbel fitting parameters and wellness of fit criteria

Data set	Gumbel coefficients		Wellness of fit parameters			
	a	w	r^2	F	n	F_{crit} 0.01
6-day LS	0.00044	2,237	0.92	338	31	7.59
8-day LS	0.00044	11,705	0.96	778	33	7.52
6-day LT	0.00056	9,161	0.92	426	39	7.37
8-day LT	0.00050	11,682	0.93	444	36	7.39

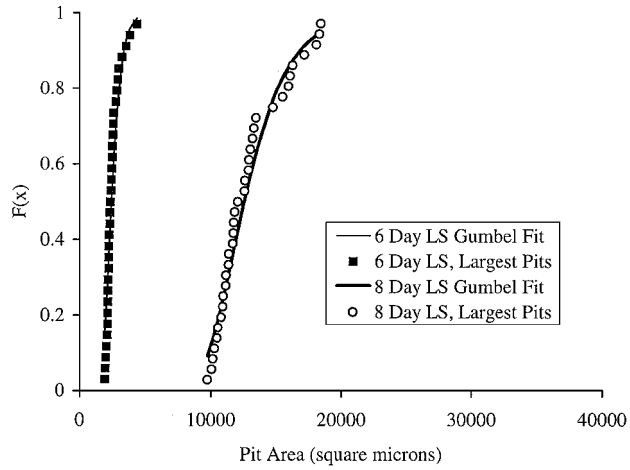

Fig. 5 Extreme-value plots of pit area with Gumbel fits: LS specimens.

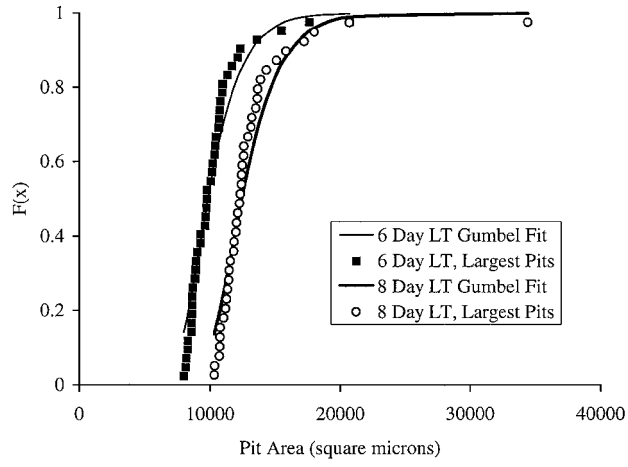

Fig. 6 Extreme-value plots of pit area with Gumbel fits: LT specimens.

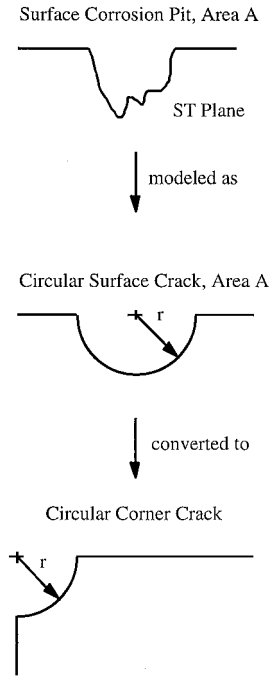

Fig. 7 Schematic of pit modeling procedure on the ST plane.

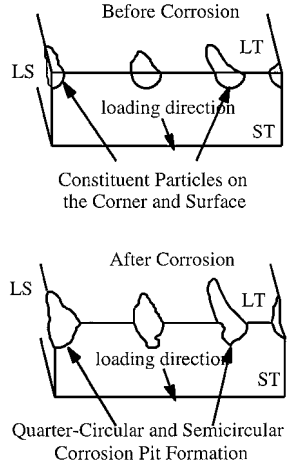

Fig. 8 Schematic illustrating corner and surface pit formation from constituent particles.

Physically, the model is based on the microstructure of the sheet material as defined by the rolling process during manufacture. This process elongates constituent particles in the rolling direction and presents elongated and flattened particles on the LT plane and cigar-shaped particles on the LS plane. Viewed from the ST plane, the particles near the edges appear semicircular. When fatigue specimens are manufactured through milling and mechanical polishing operations, the projections of constituent particles on the LT and the LS surfaces, as viewed from the ST plane, will appear semicircular except on the corners. The corners have particles that are partially polished away from both the LT and the LS surfaces, and the projections on the ST plane appear quarter circular. The corrosion pits form at the constituent particles.[1] Because the particles located at the corners were from the same distribution as those located on the surface, the corresponding corrosion pits that formed at each location should be of the same size distribution as that of the particles. Therefore the radii calculated from the assumed semicircular surface pits should be roughly equal to the radii of the quarter-circular corner pits, as schematically illustrated in Fig. 8.

FASTRAN II Fatigue Crack Growth Structural Analysis Program

FASTRAN II is a fatigue crack growth computer code developed by J. C. Newman at NASA Langley Research Center.[12,13] The code incorporates an effective stress crack growth model that accounts for crack closure. The short-crack growth behavior for which short cracks grow faster than long cracks is also incorporated into the code by the Dugdale closure model. The long-crack growth region is a typical Paris crack growth model, except that the effective stress is used to account for crack closure and stress ratio effects.

The closure crack growth model in the FASTRAN II code was validated in the AGARD studies. Material constants for crack growth models are incorporated into the code for 2024-T3 and 7075-T6 aluminum alloys, Ti–6Al–4V titanium alloy, and 4340 steel. Also included in the code are stress-intensity-factor solutions for semicircular and elliptical flaw shapes.

In the AGARD studies Newman found that fracture mechanics applies to short-crack growth behavior. Cracks were also observed to form very early in the life and the total life can be considered to be the life that is due to crack growth.

Results

Fatigue Testing Results

All 6-day LS and three of nine 8-day LS specimens were tested at a maximum stress of 220 MPa. Fatigue cracks nucleated from single pits in each 6-day LS specimen. A typical nucleating 6-day LS pit is illustrated in Fig. 9. Multiple nucleation sites were observed for 8-day LS specimens tested at 220 MPa. The maximum stress was reduced to 200 MPa for the remaining 8-day LS specimens, which resulted in nucleation from single pits. Only experimental data from the 8-day LS specimens tested at a maximum stress of 200 MPa were used to validate the probabilistic model. All 6-day LT specimens were tested at a maximum stress of 220 MPa, and six of eight 8-day LT specimens were tested at a maximum stress of 200 MPa, again because of multiple nucleation sites observed when testing at a maximum stress of 220 MPa. A typical nucleating 6-day LT pit is illustrated in Fig. 10. One 6-day and two 8-day LT specimens failed at the radii in uncorroded regions. Therefore the experimental results from seven 6-day LT and four 8-day LT specimens were used to verify the probabilistic model.

The average experimental life to fracture for the 6- and the 8-day LS specimens was 267,322 and 180,017 cycles, respectively. The average nucleating pit areas for the 6- and the 8-day LS specimens were 2519 and 24,262 μm^2, respectively. In every 6- and 8-day LS specimen, cracks nucleated from pits on the LS surface; corner crack formation was not observed. The average experimental life to fracture for the 6- and the 8-day LT specimens was 195,722 and 373,515 cycles, respectively. The average nucleating pit area for the 6- and the 8-day LT specimens was 13,295 and 17,988 μm^2, respectively. In five of seven 6-day and all 8-day LT specimens, fatigue cracks nucleated from pitting at the corners; the two remaining 6-day LT specimens nucleated cracks from pits in close proximity to a corner.

The experimental and analytical results are presented in Tables 3–6. Included in these tables are, for each specimen, the area of the crack initiating pit, the initial crack length a_i, and the aspect

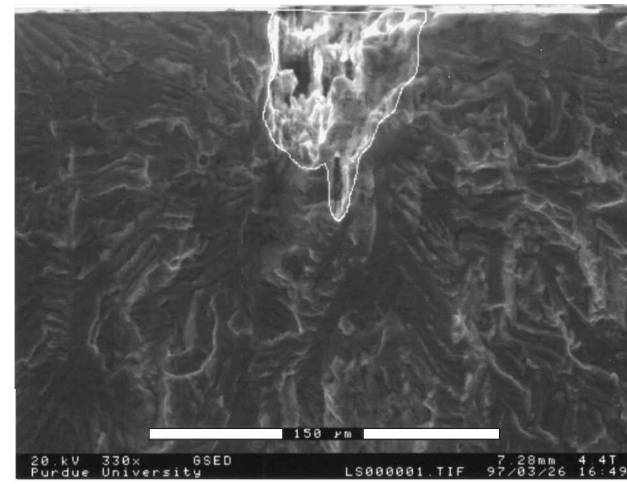

Fig. 9 ESEM micrograph of the nucleating pit for 6-day LS specimen 3 (nucleating pit outlined).

Table 3 Experimental results and life comparison: 6-day LS tests

Specimen number	S_{max}, MPa	Pit area, mm^2	Length a_i ($\times 10^{-5}$), m	Aspect ratio c/a	Experimental life cycles	Analytical life cycles	Difference, percent
1	220	892	2.38	0.68	306,086	460,920	−50.6
2	220	4,031	5.07	0.36	239,328	211,840	11.5
3	220	2,599	407	0.57	240,893	259,578	−7.76
4	220	629	200	0.97	277,102	650,280	−74.2
5	220	1,917	3.49	1.2	316,735	300,122	5.25
6	220	2,016	3.58	0.41	276,472	292,895	−5.94
7	220	2,284	3.81	0.78	277,202	275,902	0.47
8	220	1,978	3.55	0.61	275,820	295,616	−7.18
9	220	6,321	6.34	0.21	196,257	172,912	11.9

Table 4 Experimental results and life comparison: 8-day LS tests

Specimen number	S_{max}, MPa	Pit area, mm^2	Length a_i ($\times 10^{-4}$), m	Aspect ratio c/a	Experimental life cycles	Analytical life cycles	Difference, percent
1	200	23,522	1.22	1.5	178,570	141,136	20.96
2	200	22,929	1.21	2.1	177,595	142,679	19.66
3	200	25,997	1.29	1.4	181,624	135,340	25.48
4	200	22,508	1.20	1.1	188,914	143,802	23.88
5	200	26,017	1.29	1.1	154,739	135,314	12.55
6	200	24,602	1.25	1.3	198,659	138,503	30.28

Table 5 Experimental results and life comparison: 6-day LT tests

Specimen number	S_{max}, MPa	Pit area, mm^2	Length a_i, m	Aspect ratio c/a	Experimental life cycles	Analytical life cycles	Difference, percent
1	220	13,687	9.33E−05	1.6	124,718	126,884	−1.7
2	220	10,761	8.28E−05	0.58	351,018	140,805	59.9
3	220	19,828	1.12E−04	2.8	108,014	108,594	−0.5
4	220	16,719	1.03E−04	1.4	155,409	116,545	25.0
5	220	10,348	8.12E−05	1.2	127,081	143,227	−12.7
6	220	11,599	8.59E−05	1.7	152,124	136,300	10.4
7	220	10,124	8.03E−05	1.4	351,689	144,609	58.9

Table 6 Experimental results and life comparison: 8-day LT tests

Specimen number	S_{max}, MPa	Pit area, mm^2	Length a_i, m	Aspect ratio c/a	Experimental life cycles	Analytical life cycles	Difference, percent
1	200	18,025	1.07E−04	0.96	384,360	161,128	58.1
2	200	15,681	9.99E−05	2.2	422,076	171,591	59.4
3	200	12,635	8.97E−05	2.4	459,488	189,402	58.8
4	200	25,610	1.28E−05	1.4	228,135	137,943	39.5

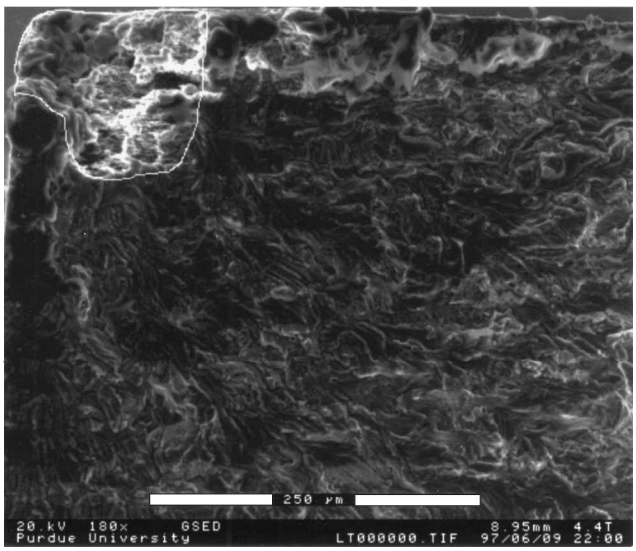

Fig. 10 ESEM micrograph of the nucleating pit located at the corner for 6-day LT specimen 3B (nucleating pit outlined).

ratio c/a. Also included are the experimental lives compared with the analytical lives determined with the FASTRAN life prediction with an initial crack area equal to that of the observed initiating pit size.

Results of the Probabilistic Model

The probabilistic model used a Monte Carlo simulation that randomly selected 1000 pit areas from each of the extreme-value distributions. From the experimental results regarding corner cracks vs surface cracks, the pit areas were modeled as circular corner cracks for the LT specimens and semicircular surface cracks for the LS specimens from which fatigue lives were predicted. The predicted and the experimental fatigue life data were sorted according to longest lives and plotted as the predicted and the experimental cumulative distribution functions (CDFs) illustrated in Figs. 11 and 12 for the LS and the LT specimens, respectively.

The probabilistic model predicted a distribution of fatigue lives within 19 and 22% of the experimental cumulative distributions for the 6- and the 8-day LS specimens, respectively. In addition, the model predicted a distribution of fatigue lives for the 6-day LT specimens that was within 23% of five experimental points and within 55% of the two remaining experimental points that comprised the

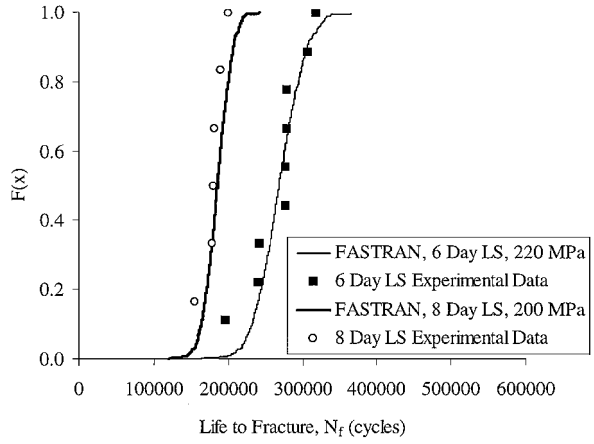

Fig. 11 Predicted and experimental CDFs of life to fracture for 6- and 8-day LS specimens.

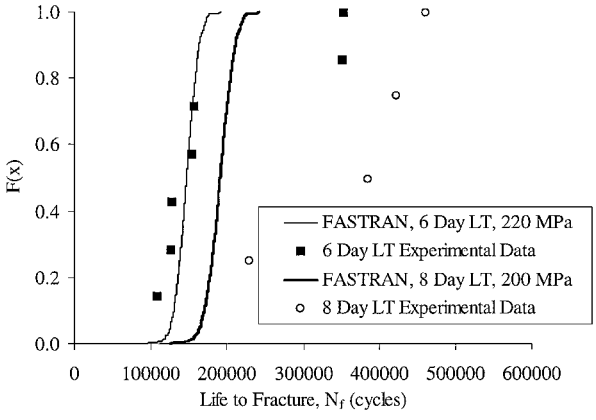

Fig. 12 Predicted and experimental CDFs of life to fracture for 6- and 8-day LT specimens.

6-day LT experimental cumulative distribution of fatigue lives. Finally, the analytical CDF of life to fracture consistently underpredicted the experimental CDF for the 8-day LT specimens and was within 53% of the experimental CDF.

Discussion of the Probabilistic Model

Overall, the probabilistic model predicted reasonable distributions of fatigue lives for the LS specimens and for the 6-day LT specimens. The predicted distribution of fatigue lives for the 8-day LT specimens was less accurate and may be due to microstructural effects. It is hypothesized that the microstructure of the aluminum sheet and the aspect ratio of the 8-day LT pits may play a role in the discrepancies. First, the 8-day LT nucleating pits were mostly characterized by broad (in the transverse direction) and rounded pits, as illustrated in the ESEM micrograph of the fracture surface of Fig. 13. By contrast, most of the 6-day LT pits were less broad and more pointed, as illustrated in Fig. 14. The result of these differences in aspect ratio from the assumed initial circular crack is that the crack growth would be slower in the short direction.

The FASTRAN II crack growth model was developed from data for crack propagation into the LS plane, whereas the crack propagation rate into the LT plane has not been measured; however, it is expected to be slower than that for the LS plane. When a crack grows in the short direction (through thickness), it must propagate through flattened or pancakelike grains formed during the rolling process in manufacturing of the sheet material. Therefore the crack growth rate into the LT plane through nonhomogenous material is expected to be significantly lower than that into the LS plane. Since the crack growth rate for the LS plane was used for both planes, this could account for the longer experimental lives than the predicted lifes for the 8-day LT specimens. In addition, the wide shallow pits for the LT corroded specimens are due to the distribution of the constituent particles from the rolling process. These particles are lined up in

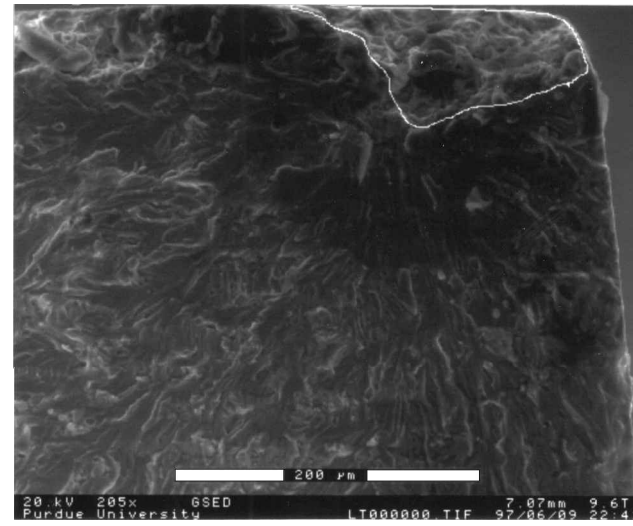

Fig. 13 ESEM micrograph of the nucleating pit for 8-day LT specimen 6B (nucleating pit outlined).

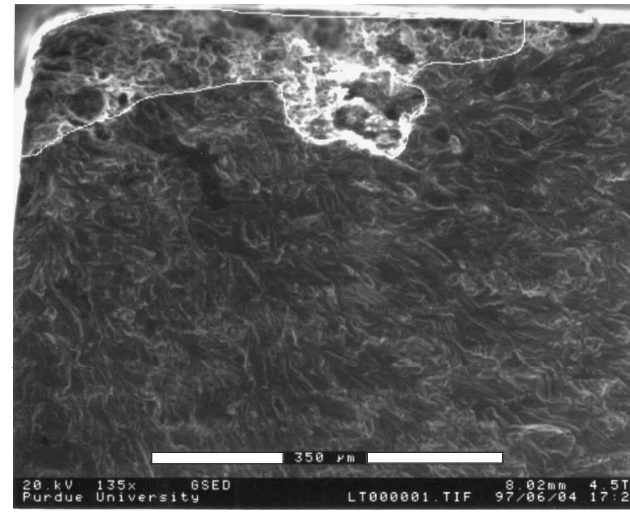

Fig. 14 ESEM micrograph of the nucleating pit for 6-day LT specimen 7 (nucleating pit outlined).

the rolling direction (into the ST plane). Corrosion pits in 2024-T3 are formed by the environment's attacking the aluminum around the cathodic particles (Al–Cu–Fe–Mn) [Eq. (3)]. Only a few particles are lined up through the pancake grains and therefore only shallow pitting occurs.

Although the probabilistic model appears to generate reasonable distributions of fatigue lives, the inclusion of additional fatigue testing data may well shift or change the shape of the experimental CDFs. Therefore the claim that the model functions reasonably well is subject to the assumption that additional fatigue testing data would not greatly alter the experimental CDFs. It is also important to note that the 6-day LS extreme-value distribution of pit area from which the initial crack areas were selected by the Monte Carlo simulation did not include pit areas as small as two of those found to nucleate cracks in the 6-day LS experiments. The predicted cumulative distribution of fatigue lives reflects the assumption that all fatigue cracks would nucleate from pits consistent with the largest 10% measured. Therefore, were the two smaller pit areas included in the Gumbel distribution, the predicted cumulative distribution of fatigue lives would be shifted to the right and would not match the experimental distribution as well for the 6-day LS CDF illustrated in Fig. 11.

Conclusions

The most significant conclusions of this work are as follows:

1) The largest pit areas were well modeled by type I extreme-value distributions.

2) Except for two 6-day LS experiments, critical fatigue cracks nucleated from corrosion pits that were among the largest 10% of those measured.

3) Slower crack growth rate in the short direction may be a factor in the underprediction of fatigue lives for two of the 6-day LT specimens and all of the 8-day LT specimens.

4) The probabilistic model predicts reasonably accurate distributions of fatigue lives for both 6- and 8-day LS specimens and the 6-day corroded LT specimens.

It should be noted that the relatively small sample sizes could significantly affect the extreme-value pit size distributions for both the experimental and the predicted distribution cumulative functions.

Acknowledgment

This research was sponsored by the U.S. Air Force Office of Scientific Research under Grant F49620-93-1-0377.

References

[1]Chen, G. S., Gao, M., Harlow, D. C., and Wei, R. P., "Corrosion and Corrosion Fatigue of Airframe Aluminum Alloys," *FAA/NASA International Symposium on Advanced Structural Integrity Methods for Airframe Durability and Damage Tolerance*, NASA CP 3274, 1994, pp. 157–173.

[2]Burynski, R. M., Chen, G. S., and Wei, R. P., "Evolution of Pitting Corrosion in a 2024-T3 Aluminum Alloy," *Proceedings of 1995 International Mechanical Engineering Congress and Exposition*, AD. Vol. 47, American Society of Mechanical Engineers, New York, 1995, pp. 175–183.

[3]Kondo, Y., "Approach to Quantitative Evaluation of Corrosion Fatigue Crack Initiation Condition," *Nippon Kikai Gakkai Ronbunshu*, Vol. 57, No. 537, 1991, pp. 1057–1061 (in Japanese).

[4]Laz, P. J., and Hillberry, B. M., "Fatigue Life Prediction from Inclusion Initiated Cracks," *International Journal of Fatigue*, Vol. 20, No. 4, 1998, pp. 263–270.

[5]"Test Methods of Tension Testing of Metallic Materials," ASTM E8-87a, Vol. 3.01, American Society for Testing and Materials, Philadelphia, PA, 1998, pp. 121–136.

[6]Virkler, D. A., Hillberry, B. M., and Goel, P. K., "The Statistical Nature of Fatigue Crack Propagation," *Journal of Engineering Materials and Technology*, Vol. 101, No. 2, 1979, pp. 148–153.

[7]"Evaluating Stress Corrosion Cracking Resistance of Metals and Alloys by Alternate Immersion in 3.5% Sodium Chloride Solution," *American Society for Testing Materials Standards*, ASTM 644-88, Vol. 3.02, American Society for Testing and Materials, Philadelphia, PA, 1998, pp. 193–196.

[8]"Preparing, Cleaning, and Evaluating Corrosion Test Specimens," ASTM G1-90, Vol. 3.02, American Society for Testing and Materials, Philadelphia, PA, 1990, pp. 39–45.

[9]IMIX, Ver. 7, Princeton Gamma-Tech, Princeton, NJ, 1994.

[10]NIH Image, Ver. 1.63, National Institutes of Health, Washington, DC, 1996.

[11]Newman, J. C., Jr., and Raju, I. S., *Stress Intensity Factors Handbook*, edited by Y. Murakami, Vol. 2, Pergamon, New York, 1987, pp. 712–715.

[12]Newman, J. C., Jr., "FASTRAN II: A Fatigue Crack Growth Structural Analysis Program," NASA TM 104159, 1992.

[13]Newman, J. C., Jr., and Edwards, P. R., "Short-Crack Growth Behavior in an Aluminum Alloy—An AGARD Cooperative Programme," AGARD Rept. 732, 1988.

A. M. Waas
Associate Editor